HHS Public Access

Author manuscript

Lancet Haematol. Author manuscript; available in PMC 2021 March 01.

Published in final edited form as:

Lancet Haematol. 2020 March ; 7(3): e259–e269. doi:10.1016/S2352-3026(20)30003-X.

Imaging haemopoietic stem cells and microenvironment dynamics through transplantation

Kirsten M Williams,

Department of Pediatrics, Emory University and the Children's Healthcare of Atlanta, Atlanta, GA, USA; Division of Blood and Marrow Transplantation, AFLAC Cancer and Blood disorder Center, Atlanta, GA, USA

Jennifer Holter Chakrabarty

Department of Medicine, Division of Marrow Transplantation and Cell Therapy, Stephenson Cancer Center, Oklahoma City, OK, USA

Abstract

Understanding the subclinical pathway to cellular engraftment following haemopoietic stem cell transplantation (HSCT) has historically been limited by infrequent marrow biopsies, which increase the risk of infections and might poorly represent the health of the marrow space. Nuclear imaging could represent an opportunity to evaluate the entire medullary space non-invasively, yielding information about cell number, proliferation, or metabolism. Because imaging is not associated with infectious risk, it permits assessment of neutropenic timepoints that were previously inaccessible. This Viewpoint summarises the data regarding the use of nuclear medicine techniques to assess the phases of HSCT: pre-transplant homoeostasis, induced aplasia, early settling and engraftment of infused cells, and later recovery of lymphocytes that target cancers or mediate tolerance. Although these data are newly emerging and preliminary, nuclear medicine imaging approaches might advance our understanding of HSCT events and lead to novel recommendations to enhance outcomes.

Introduction

The biology of cellular homing, settling, and recovery that underpins haemopoietic stem cell transplantation (HSCT) has been difficult to study. HSCT involves, firstly, the reduction or ablation of marrow, followed by the infusion of healthy haemopoietic stem cells, which leads to the recovery of normal donor haemopoiesis and lymphopoeisis, as evidenced by the presence of mature peripheral blood cells. Aplasia occurs following the ablation of the haemopoietic compartment and before the re-establishment of donor haemopoiesis. Despite

Correspondence to: Dr Kirsten M Williams, Department of Pediatrics, Emory University and the Children's Healthcarel of Atlanta, Atlanta, GA 30322, USA, kwill99@emory.edu.

Contributors

KMW and JHC jointly performed the literature search on July 5, 2019.

Both authors reviewed literature, co-wrote and edited the entire manuscript, created and chose figures for the manuscript, and co-created the table.

Declaration of interests

We declare no competing interests.

being the gold standard, marrow biopsies to evaluate this stage of the process are associated with high risk of infection and bleeding during neutropenia, thus limiting their use at early time-points after infusion of donor cells. Furthermore, the marrow compartment is large and includes poorly accessible sites (eg, axial spinous medullary spaces) and is highly heterogeneous. There are simultaneously sites of marrow loss, dysplasia, and of recovery, and this heterogeneity leads to sampling bias and incomplete information about marrow reconstitution from biopsies. Imaging potentially provides a valuable method to comprehensively and painlessly evaluate the completeness of marrow ablation, and the migration, settling, and repopulation of infused cells without incurring infection and bleeding risks.

Radiographic imaging can diagnose alterations within the marrow, such as leukaemic infiltration. However, nuclear medicine affords information about the dynamic function and activity of the marrow compartment by using a low dose radioactive isotope that is internalised and then detected as an emission by an external source. These nuclear medicine imaging techniques can identify the metabolic, proliferative, and transcriptional activities within marrow cells using precise radiolabeled molecules. Radioisotopes can label specific cells (eg, haemopoietic stem cells) to monitor trafficking or identify genetically modified cells to show activity or proliferation. Alternatively, radioisotopes can be systemically infused and target cell populations or show the differences in metabolism between cell populations on the basis of uptake. The US Food and Drug Administration (FDA)-approved nuclear medicine test, ^{18}F-fluorodeoxyglucose (^{18}F-FDG) PET, is widely used to diagnose and stage solid tumours and other nodal diseases, such as lymphoma.[1,2] In Hodgkin lymphoma, FDG PET staging has improved risk-adapted treatment algorithms as compared with CT alone.[3]

In this Viewpoint, we describe nuclear medicine methods for marrow interrogation using in vivo, in vitro, and ex vivo tagging of cellular components to identify processes within the marrow that are otherwise difficult or impossible to assess (table). These nuclear medicine evaluations included the one FDA-approved radioisotope for marrow studies (^{18}F-FDG) and many investigational agents in human and animal models. The radioisotopes are classified by the cellular processes that are visualised within the marrow compartment (ie, cellular proliferation evaluated by labelled metabolites used in cell division, cellular metabolism evaluated by glucose uptake, and static identification or localisation evaluated by labelling particular cell subsets). We discuss the stages of HSCT from the perspective of the information garnered from nuclear medicine imaging; these stages include: (1) normal haemopoiesis, (2) reduced haemopoiesis or aplasia, (3) haemopoietic repopulation or recovery, (4) sequelae of both healthy and disordered recovering haemopoiesis, and the resulting immunosurveillance or immunotherapy.

Imaging of normal haemopoiesis (pre-HSCT)

Animal studies have used nuclear medicine imaging to identify healthy marrow activity, including ^{18}F-FDG, a marker of cellular metabolism, in a murine model.[14,38] ^{18}F-FDG is a glucose analogue tagged with fluorine-18 and, although ^{18}F-FDG is incorporated by all cells, hypermetabolic cells (eg, proliferating or activated cells) show increased uptake of this

radiotracer. ^{18}F has also been tagged to thymidine ^{18}F-fluorothymidine (^{18}F-FLT), which identifies cellular proliferation of HSCs, lymphocytes, and cancer cells using the thymidine salvage pathway. Using ^{18}F-FLT, the architecture of feline marrow was defined.[13] Other animal studies have transduced nonhuman primate cells with a lentiviral vector expressing a PET reporter gene (the mutant viral herpes simplex virus type 1–thymidine kinase [HSV1-TK] gene labeled with 5-^{76}Br-bromo-2-fluoro-2-deoxyuridine [^{76}Br-FBAU]) and green fluorescent protein (GFP) for infusion into irradiated rhesus macaques, in which they modelled recovery of normal haemopoiesis and tracked marrow proliferation.[25] GFP was detectable by flow cytometry and allowed for identification of all progeny in the circulation.[25] ^{64}Cu-labelled liposomes were used in animal studies to image the marrow and splenic compartments; they were also proposed as drug delivery system; however, further study is required to define stability of delivery in the context of chemotherapy and radiation.[26] In humans, ^{18}F-FLT and ^{18}F-FDG have both been used clinically to evaluate healthy haemopoiesis throughout the medullary spaces, in terms of proliferative and metabolic activity, respectively.[34,47] Human studies of ^{18}F-FDG have highlighted that haemopoiesis might be substantially influenced by inflammation,[29,33] and must also be carefully evaluated in the setting of growth factor administration, such as erythropoietin and GCSF.[35,48] Studies of normal haemopoiesis in adult humans using ^{18}F-FLT show that marrow primarily resides in the axillary skeleton, with proximal humerus and femur activity, and that extramedullary activity in the spleen and liver does not occur under normal circumstances.[33-35]

Imaging cytoreduction (preparative HSCT stage)

Although only a few imaging studies have been done to evaluate cytoreduction during the preparative stage of HSCT, many studies have evaluated the effects of chemotherapy or radiation on the marrow space, informing this part of HSCT. Using infused ^{18}F-FDG in murine models, the reduction of haemopoiesis following chemotherapy with gemcitabine or radiation was visualised, and then confirmed by peripheral counts and splenic immunohistochemistry.[12,14,49] The doses of radiation that were insufficient to eradicate haemopoietic progenitors were shown in this model, with recovery of haemopoiesis visualised within 72 h of radiation using ^{18}F-FDG.[14] ^{18}F-FLT was used to show the full myeloablative reduction of marrow signalling to null in a rat model (figure 1).[12] Clinically, radiation marrow reduction has been evaluated using both ^{18}F-FLT and ^{18}F-FDG, showing proliferative and metabolic activity, respectively.[32,39,41,50] These studies suggest that nuclear medicine techniques could potentially be used to better understand the potency of cytoreduction, informing the radiation or chemotherapy doses needed to achieve effective marrow ablation.

Imaging engraftment, homing, and proliferation (post-HSCT)

The early period after HSCT involves homing of HSCs to the marrow niches, the settling of cells within these niches, and the rapid proliferation of these stem cells and their progenitors. Historically, this timeframe was poorly studied because of both the inherent risks of biopsies and the inability to detect circulating cells early. Cells are not detectable until weeks after HSC infusion. Successful donor haemopoiesis is correlated with engraftment, defined as 3 days of >500 cells per dL in the peripheral blood; figure 2). Imaging has successfully

evaluated this time-frame in both animal models and, since 2012, in patients who have received HSCT.

Although HSCs can be directly labelled with ^{18}F-FDG in vitro and adoptively transferred into rodents, labelling is toxic to the stem cells, thereby compromising engraftment.[6] By contrast, HSCs and mesenchymal stem cells could be labelled with ^{64}Cu-pyruvaldehyde-bis (N4-methylthiosemicarbazone) (^{64}Cu-PTSM) in a rhesus monkey model; in this study, the label was non-toxic and did not affect engraftment, and cells could be easily traced using a microPET scanner.[9] Similarly, ^{89}Zr radiolabelling of HSCs did not affect their survival and gradually released the radiotracer, permitting PET identification after adoptive transfer into swine.[7] In addition, intrabone adoptive transfer experiments of the ^{89}Zr-HSCs showed that the HSCs were better retained in the medullary space when a lower infusion rate was used.[7] Collectively, these data suggest that in vitro cellular labelling, followed by adoptive transfer, can show HSC homing and early engraftment.

HSCs have also been genetically modified to incorporate reporter genes that permit specific imaging using PET scanning. For example, in murine HSCs, a gene within the nucleoside salvage pathway was specifically altered and incorporated human deoxycytidine kinase containing three amino acid substitutions (*hdCK3mut*) and imaged with the PET probe 1-(2-deoxy-s-^{18}fluoro-β-L-arabinofuranosyl)-5-methyluracil (^{18}F-L-FMAU).[4] After myeloablation, the genetically modified HSCs were adoptively transferred into mice, and showed durable engraftment by PET and CT 1 month later. Persistence of the reporter gene was evident after 6 months in mature haemopoietic cell populations without evidence of autoimmune clearance.[4] Similarly, HSCs were transduced with a reporter gene that shows proliferation using the thymidine salvage pathway HSV1 TK-EGFP-FLuc TGL, including fluorescence (enhanced GFP), bioluminescence (firefly luciferase), and radiotracer (^{131}I-2'-fluoro-2'-deoxy-1-beta-d-arabinofuranosyl-5-iodouracil[FIAU]) reporters.[5] Bioluminescence was used to evaluate HSC proliferation and early settling after transplantation. Proliferation was minimal in the first 2 days, consistent with cell analysis after sacrifice at these time points, followed by a significant increase in proliferation 6 days after transplantation. CT showed that HSCs homed to extremities, as well as the axial skeleton, after adult murine HSCT.[5] HSCs have also been transfected with a viral vector to evaluate proliferation using imaging; specifically this method used HSV1-TK^{18}F-FIAU.[8] The transduced cells successfully showed the proliferative activity and migration of HSCs following adoptive transfer into swine.[8] Thus, various genetic modification of HSCs have shown the processes of HSC homing, differentiation, and persistence of transfused cells into specific medullary spaces, including those that do not typically include haemopoiesis in adulthood—the extremity.

In addition to labelling HSCs before infusion, imaging approaches have used systemic radiotracers that are incorporated by HSCs in vivo to elucidate engraftment biology. Both ^{18}F-FDG and ^{18}F-FLT were used to study early haemopoietic events after transplantation in a rat model that mimics the clinical situation. Wistar Furth rats were treated with 950 cGy and imaged after syngeneic transplantation. Within only 4 days, donor marrow recovery was evident in the medullary spaces using ^{18}F-FLT; detection by ^{18}F-FLT preceded pathological marrow and peripheral blood cellular confirmation by more than 5 days, providing greater

resolution of the marrow compartment.[38] The intensity of ^{18}F-FLT could be objectively evaluated by using signal thresholds as a fraction of the injected dose. The ^{18}F-FLT signal intensity increased by 5 times between the image after myeloablation and the image 4 days after transplantation, indicative of the rapid marrow cell expansion.[38] By contrast, the ^{18}F-FDG signal decreased in this timeframe, consistent with reduced inflammation but not indicative of the newly infused cell expansion. This observation suggests that use of ^{18}F-FLT might be a more accurate method to evaluate this early time frame after HSCT than ^{18}F-FDG.[38] The trafficking of marrow cells to non-irradiated sites first, and then to myeloablated sites after, termed an abscopal effect, was also shown using ^{18}F-FLT in a murine bone marrow transplant model.[12] These data suggest that an increase in ^{18}F-FLT signal intensity might present an opportunity to identify subclinical engraftment, showing HSC expansion in the early HSCT period, and could have clinical implications.

In humans, the first evaluation of HSCT haemopoiesis by imaging used the standard clinical PET and CT with ^{18}F-FDG. Marrow spaces were delineated using a computer algorithm 30 days after allogeneic cord blood and allogeneic marrow or peripheral blood HSC transplantation to evaluate cell expansion in the recipient's marrow.[27] After allogeneic transplantation, the volume of expansion was six times higher than in homoeostatic adult marrow while the expansion was only three times higher after cord blood HSCT (figure 3).[27] Because the cell dose of cord blood is lower than that for other HSC products, the different levels in the bone marrow cell metabolism signal are likely to reflect greater numbers of cells settling within the marrow spaces. Moreover, because imaging occurred 30 days after HSCT infusion, the influence of the inflammatory events preceding cell infusion should be diminished. In addition, this study showed that active haemopoiesis occurred in the extremity marrow spaces in adults, reclaiming areas that are usually dormant after childhood.[27] Similarly, ^{18}F-FDG has been used to study intrabone injections of blood cord HSCs—an approach that decreases the need for newly infused cells to home to the marrow spaces, and potentially accelerates de novo haemopoiesis.[28] At 30 days after cord blood transplantation, the maximal standardised uptake volume (SUV) was higher in the injected sites (ie, iliac crests) than the axial skeleton, which was consistent with settling at the sites of direct inoculation.[28] Further, these direct intrabone cord blood infusions translated to faster platelet recovery, suggesting that removing the necessity of cord blood homing to the marrow might expedite engraftment and peripheral count recovery. These studies showed that imaging could provide valuable information regarding differences in the density of marrow settling across the human skeleton, and that the revealed biology of HSCT engraftment could potentially translate into changes in clinical practice to enhance outcomes.

Subclinical homing and marrow settling early after HSCT have been evaluated using ^{18}F-FLT imaging; the authors successfully translated their earlier bench work to a clinical protocol.[38,40] 23 patients who underwent myeloablative transplantation following a radiation preparative regimen were imaged with ^{18}F-FLT at four timepoints: the day before haemopoietic cell infusion, early after infusion (day 5–12), and at 28 days and 1 year after transplantation. At the timepoints of 28 days and 1 year, ^{18}F-FDG PET or CT was also done with ^{18}F-FLT. ^{18}F-FLT better visualised the marrow compartment subjectively compared with FDG.[40] ^{18}F-FLT was well tolerated at the early timepoints after HSCT and did not

delay recovery of peripheral blood counts—a concern with radiation exposure to newly infused HSCs—and there was no graft failures. ^{18}F-FLT SUV was significantly increased between myeloablative levels (1 day before HSCT), and 5 days after HSCT; values at early timepoints did not overlap with the higher values 28 days after infusion, showing that ^{18}F-FLT SUV could discriminate between subclinical haemopoiesis, absent haemopoiesis, and fully engrafted haemopoiesis. As expected, there was a rapid increase in SUV in the first 5 days of transplantation, consistent with rapid expansion of newly infused cells. Surprisingly, the serial ^{18}F-FLT images showed a recurring pattern of sites of cellular recovery, with cells first homing to the liver and spleen (at days 5–6), then to the thoracic medullary spaces (at days 5–12), followed by the remainder of the axial skeleton (at days 9–12), and lastly, the extremities (28 days after infusion).[40] Marrow uptake returned to basal axial skeleton sites only 1 year after transplantation (figure 4). This pattern was a previously unknown pathway of cellular recovery in adults that mimicked fetal ontogeny development of haemopoiesis.[40] The clinical implications of these data need to be further elucidated. Could ^{18}F-FLT be used to diagnose graft failure? Possibly, although the absence of graft failures in the allogeneic published study[40] precluded answering this important question. Is it possible that some transplants fail because the cells do not migrate from the liver and spleen to the medullary spaces? Data have linked splenomegaly and previous splenic haemopoiesis to delayed or failed engraftment. It is also unknown whether this pathway to cellular engraftment occurs after alternative donor transplantation (ie, cord blood or haplo-identical) or non-radiation containing preparative regimens. A clinical trial is underway to answer this query (NCT03541889). Despite these limitations, this study[40] suggests that the cellular paths followed during subclinical engraftment in humans are the same as those seen in rodent models, mimicking human ontogeny. Thus, this study showed an aspect of engraftment biology not accessible through standard invasive means because of the risk of life-threatening infections.

Imaging to show graft failure (post-HSCT)

Following HSCT, graft failure can ensue, often due to immunological rejection by resident host cells, mimicking the process of aplastic anaemia. Graft failure after HSCT caused by immunological rejection has not yet been shown by imaging; however, ^{18}F-FLT has successfully shown both a heterogeneous and reduced pattern of marrow proliferation in patients with active aplastic anaemia, and a return to homoeostatic levels in patients who had recovered.[44] Vigilance is needed in these situations in which disease processes or medications can cause confounding marker uptake, leading to false negatives or false positives. For example, GCSF and erythropoietin induce proliferation of marrow subsets and, thus, generate heterogeneous increased ^{18}F-FDG SUV that could incorrectly indicate an infiltrative or unhealthy haemopoiesis.[35,48] Such results can confound the increased uptake and heterogeneity that typify infiltrative cancer processes and in which SUV exceeds liver levels.[29,46] Marrow cellularity inversely correlates with age, and this natural reduction in SUV has been shown by ^{18}F-FDG and could be confused with emerging marrow failure.[33] ^{18}F-FLT has been used successfully to distinguish the healthy recovery of cells from haemopoietic malignancy.[43,45]

Imaging to show lymphocyte recovery and graft-versus-tumour effects

The early phase of transplantation includes recovery of natural killer cells, neutrophils, red blood cells, and platelets. Later, there is recovery of lymphocytes with de novo thymopoiesis, which is important for graft-versus-tumour effects, viral clearance, and tolerance of the allogeneic immune system. Animal models have shown that the adoptive transfer of immune cells can be imaged and show the efficacy of immunotherapy, although only few of these studies have been translated to clinical use.

Haemopoietic cells can be genetically modified and transplanted to evaluate the homing, expansion, and efficacy of immunotherapy. Human peripheral blood mobilised stem cells that have been transduced with an anti-melanoma T-cell receptor F5 and the ^{18}F-L-FMAU plus *hdCK3mut* PET probe could be shown to home to melanoma lesions and induce cytotoxic effects in a murine model.[4] Similarly, human peripheral blood stem cells have been genetically modified to target B-cell malignancy, using an anti-CD19 chimeric antigen receptor (CAR) and truncated epidermal growth factor receptor.[15] These CD19 CAR T cells have been shown to eradicate leukaemias and lymphomas that express CD19. After transplantation of CD19 CAR T cells into a murine model, treatment with ^{89}Zr-labelled cetuximab (which inhibits epidermal growth factor receptor) lysed the gene-modified cells, thereby providing a safety mechanism to deplete these cells.[52] Finally, human peripheral blood mobilised stem cells have also been transfected to generate a T-cell receptor specific for the tumour antigen NY-ESO-1, which could lyse human melanoma cells (that express NY-ES0-1 in vitro), and contained a suicide gene.[16-18,53] Without additional genetic insertions, the HSV1-TK transduced lymphocytes were shown to traffic to malignant glioma in a rat model, as well as being assessed in murine sarcoma and leukaemia models.[16,17] In these models, PET intensity localised to the tumour beds and draining lymph nodes. In the glioma model, PET intensity was consistent with MRI findings and histology.[17,52] These studies provide proof of principle that imaging can show the efficacy of immunotherapy. This work was translated to humans in a study that used human cytotoxic T cells that were transfected with an HSV1-TK and interleukin-13 (IL-13) CAR, whereby the cells homed to glioblastoma in humans, as shown by colocalisation by MRI, PET, and CT.[53]

In addition to genetic modification of cells, localisation of the cells of interest has been accomplished through direct labelling (done before infusion), antibody detection, and systemic PET-probe exposure. In a murine transplantation model, the lymphoid recovery of CD4 and CD8 T cells within primary and secondary lymphoid organs was shown with ^{89}Zr.[22] Labelled T cells have shown T-cell tumour homing and lysis in vivo. In a rodent orthotopic glioma model, ^{111}In-labelled human cord blood cytotoxic T cells quickly targeted the tumour bed and increased signal intensity for 24 h.[19] To identify anti-cancer T cells, the variable fragment of an antibody (diabody or minibody) was labelled with either ^{M}Cu, or ^{18}F, or using maleimide-desferrioxamine for ^{89}Zr (figure 5).[20,22] A supportive influx of host of macrophages and dendritic cells have been shown by labelled variable fragments in a murine melanoma model using regions that recognise MHC-class II and CD11b.[20] The cytoreductive effects of chemotherapy have been shown by labelled chemotherapy agents, such as ^{18}F-clofarabine, in the marrow and lymphoid organs in healthy volunteers.[21] In a patient with a paraganglioma, ^{18}F-clofarabine showed segmental loss of activity within the

marrow after radiation treatment.[21] Finally, nuclear medicine agents can label tumour cells as well. Pentixafor, a PET imaging reagent targeting CXCR-4, showed patient-derived leukaemias in xenograft murine models.[23] Endoradiotherapy with ^{177}Lupentixather was used to treat the leukaemias in a xenograft model, and subsequently in three patients with acute myeloid leukaemia; imaging showed effective leukaemia clearance.[23] Collectively, these data suggest that nuclear medicine imaging might provide a unique opportunity to assess the trafficking, proliferation, and efficacy of immunotherapies, both in animal models and in the clinic.

Imaging to show trafficked lymphocytes (post-HSCT and in graft-versus-host disease)

As of 2020, work to show healthy lymphoid recovery and tolerance is scarce; there is one study showing thymus recovery after chemotherapy,[55] although there are more studies showing the influence of intolerance or the alloimmune effects of graft versus host disease (GVHD). Murine models of transplantation have used nuclear medicine imaging to evaluate graft-versus-host disease. The activated and proliferating T cells mediating subclinical GVHD have been shown in spleen and lymph nodes using ^{18}F-FDG, ^{18}F-FLT, 2′-deoxy-2′-^{18}Fluoro-9-β-D-arabinofuranosylguanine (^{18}F-AraG), and a ^{64}Cu-labelled minibody against HLA-DR.[10,11,24,37] In humans, ^{18}F-FDG has confirmed chronic GVHD myositis and was specifically correlated with gastrointestinal tract GVHD with increased uptake in this site.[36,37] Although there are few studies, they suggest that imaging could offer opportunities to both identify subclinical GVHD and interrogate the pathobiology predating the clinical manifestations.

Discussion

This Viewpoint focuses on the nuclear medicine evaluations of the biology underpinning the stages of HSCT. Studies in healthy homoeostatic haemopoiesis permit differentiation of cellular reduction and ablation due to the preparative regimen. The loss of haemopoiesis within the medullary spaces has been shown using both ^{18}F-FLT and ^{18}F-FDG in animal models and humans, with systemic agents that show proliferation and metabolism (respectively) of the cells. Although ^{18}F-FDG is non-specific, ^{18}F-FLT better discerns the marrow events because it is restricted to HSCs, lymphocytes, and cancer cells. ^{18}F-FDG, ^{18}F-FLT, and other radioisotopes might be valuable for identifying the potency of haemopoietic cell reduction in various preparative regimens, for informing the minimum dose needed to eradicate haemopoiesis, and for permitting donor engraftment; however, these have yet to be studied systematically.

The evaluation of subclinical, early homing, and settling of infused marrow cells has used systemic agents and in vitro radiolabelling with ^{64}Cu-PTSM or ^{89}Zr before adoptive transfer in animal models to track the HSC pathway to engraftment. Transduced and labelled HSCs have also yielded insight into the HSC homing patterns, proliferation, and subsequent differentiation to mature blood components. The systemic infusion of ^{18}F-FLT and ^{18}F-FDG have been translated clinically to evaluate subclinical haemopoiesis. ^{18}F-FDG showed a pattern of haemopoiesis that reclaimed previously dormant sites of haemopoiesis from

childhood (ie, the extremities) after transplantation. This work was extended by the use of ^{18}F-FLT at earlier timepoints after HSC infusion, showing a previously unknown pattern of cellular engraftment that recapitulated fetal ontogeny. Although this work suggests that ^{18}F-FLT could be used to identify subclinical engraftment and, therefore, graft failure, the absence of patients with this complication precluded evaluation. Further work with nuclear medicine imaging during HSCT might identify whether this pattern is followed by all transplantation procedures, including alternative donors such as cord blood or haploidentical recipients. Future studies of these radioisotopes and other novel agents will need to investigate the influence of co-administered growth factors, as these can influence the cellular proliferation and metabolism of early marrow recovery. In addition, marrow imaging could predict the time remaining until clinical engraftment and could help to make treatment decisions to accelerate marrow recovery.

The final phase of HSCT, including lymphoid reconstitution, tumour eradication, and host tolerance, might also benefit from nuclear medicine imaging evaluations. The adoptive transfer of transduced T cells that have been labelled with various PET probes have successfully eradicated brain tumours in vitro, and melanoma and B-cell tumours in murine models. These labelled T cells can show proliferative activity of newly infused cells, and could inform methods to enhance the eradication of tumours. In addition, direct labelling of leukaemic cells has showed the effects of immunotherapy by targeting CXCR4. Collectively, nuclear medicine studies have shown the trafficking, proliferation, and efficacy of immunotherapies in animal models and in a clinical context. As this field continues to expand, the information garnered from non-invasive, comprehensive images could benefit future immunotherapy protocols by showing deficits in cell number, homing or proliferation, and showing the efficacy of infused therapies. Similarly, the use of ^{18}F-FDG imaging in GVHD could offer novel opportunities to enhance diagnosis, prognosis, and response in a relapsing remitting disease that is notoriously difficult to assay with available modalities.

Data are scarce for all of these nuclear medicine imaging modalities, constraining the ability to compare or recommend particular strategies. In addition, although multiple search terms were attempted to yield the largest relevant dataset to initiate the review process, the expansive variety of search terms used in this field was a challenge and might have led to incomplete data. In addition, there are inherent limitations of the imaging modalities. Direct labelling in vitro yields specific information about particular cell populations and their progeny, but is shortlived and can be toxic to the cells, thereby limiting the potential for these findings to be translated into clinical use. Similarly, gene transduction of ex vivo cell populations is specific to the population of interest but requires genetic insertions with the inherent potential for leukemogenesis or immune-mediated rejection, thereby limiting clinical use. Labelled minibodies can yield specific information about populations without these risks, although the particular adoptive transferred cells cannot be identified. Finally, systemic radioisotopes are already in clinical practice, but can be non-specific and do not label the specific cells infused.

Conclusion

These data show that nuclear medicine studies can yield information about cellular homing, settling, activity, tumour lysis, immune attack of healthy tissues, and engraftment and recovery of lymphoid populations after HSCT that is otherwise inaccessible through standard biopsies. In addition to providing information about metabolism and cell proliferation, these studies might be able to show the efficacy of particular immunotherapies and identify the causes of treatment failure. In HSCT, nuclear imaging might show aplasia in the marrow and permit facile rapid diagnosis of graft failure, and trials to investigate this are ongoing. In the setting of immunotherapy, nuclear medicine could identify why infused cells fail to eradicate tumour cells (ie, poor homing, proliferation, or inability to induce cell death despite effective targeting). As in other areas of medicine, nuclear medicine in transplantation heralds a new opportunity for understanding the underpinnings of disease and the biology of transplantation that can lead to early intervention and therapy.

Acknowledgments

Danny Morton (University of Oklahoma Health Science Center, Stephenson Cancer Center, OK, USA) provided medical editing for this manuscript. This work was supported through administrative core P30CA225520 grant obtained through the US National Cancer Institute awarded to the University of Oklahoma Stephenson Cancer Center. In addition, JHC's contributions were supported through the Oklahoma Shared Clinical and Translational Resource program through a US National Institutes of Health Grant U54GM104938. Both authors' work is in part funded by R01HL146668-01 (Multi-PI).

References

1. Kostakoglu L, Goldsmith SJ. 18F-FDG PET evaluation of the response to therapy for lymphoma and for breast, lung, and colorectal carcinoma. J Nucl Med 2003; 44: 224–39. [PubMed: 12571214]
2. Schöder H, Larson SM, Yeung HW. PET/CT in oncology: integration into clinical management of lymphoma, melanoma, and gastrointestinal malignancies. J Nucl Med 2004; 45 (suppl 1): 72S–81S. [PubMed: 14736838]
3. Spinner MA, Advani RH. Risk-adapted therapy for advanced-stage Hodgkin lymphoma. Hematology (Am Soc Hematol Educ Program) 2018; 2018: 200–06. [PubMed: 30504311]
4. McCracken MN, Gschweng EH, Nair-Gill E, et al. Long-term in vivo monitoring of mouse and human hematopoietic stem cell engraftment with a human positron emission tomography reporter gene. Proc Nat Acad Sci USA 2013; 110: 1857–62. [PubMed: 23319634]
5. Mayer-Kuckuk P, Doubrovin M, Bidaut L, et al. Molecular imaging reveals skeletal engraftment sites of transplanted bone marrow cells. Cell Transplant 2006; 15: 75–82. [PubMed: 16700332]
6. Faivre L, Chaussard M, Vercellino L, et al. 18F-FDG labelling of hematopoietic stem cells: dynamic study of bone marrow homing by PET-CT imaging and impact on cell functionality. Curr Res Transl Med 2016; 64: 141–48. [PubMed: 27765274]
7. Pantin JM, Hoyt RF Jr, Aras O, et al. Optimisation of intrabone delivery of hematopoietic progenitor cells in a swine model using cell radiolabeling with [89] zirconium. Am J Transplant 2015; 15: 606–17. [PubMed: 25656824]
8. Pei Z, Lan X, Cheng Z, et al. A multimodality reporter gene for monitoring transplanted stem cells. Nucl Med Biol 2012; 39: 813–20. [PubMed: 22336371]
9. Huang J, Lee CC, Sutcliffe JL, Cherry SR, Tarantal AF. Radiolabeling rhesus monkey CD34+ hematopoietic and mesenchymal stem cells with 64Cu-pyruvaldehyde-bis (N4-methylthiosemicarbazone) for microPET imaging. Mol Imaging 2008; 7: 1–11. [PubMed: 18384718]

10. Ronald JA, Kim BS, Gowrishankar G, et al. A PET imaging strategy to visualize activated T cells in acute graft-versus-host disease elicited by allogenic hematopoietic cell transplant. Cancer Res 2017; 77: 2893–902. [PubMed: 28572504]
11. Lee YZ, Akinnagbe-Zusterzeel E, Fowler KA, Coghill JM. 18F-3'-deoxy-3'-fluorothymidine positron emission tomography imaging for the prediction of acute graft-versus-host disease in mouse hematopoietic stem cell transplant models. Biol Blood Marrow Transplant 2018; 24: 2184–89. [PubMed: 29981461]
12. Afshar SF, Zawaski JA, Inoue T, et al. Investigating the abscopal effects of radioablation on shielded bone marrow in rodent models using multimodality imaging. Radiat Res 2017; 188: 56–65. [PubMed: 28475423]
13. Rowe JA, Morandi F, Wall JS, et al. Whole-body biodistribution of 3'-deoxy-3'-[(18) F]fluorothymidine ((18) FLT) in healthy adult cats. Vet Radiol Ultrasound 2013; 54: 299–306. [PubMed: 23464567]
14. Chen C, Yan LM, Guo KY, et al. The diagnostic value of 18F-FDG-PET/CT in hematopoietic radiation toxicity: a Tibet minipig model. J Radiat Res (Tokyo) 2012; 53: 537–44. [PubMed: 22843618]
15. Kao RL, Truscott LC, Chiou TT, Tsai W, Wu AM, De Oliveira SN. A cetuximab-mediated suicide system in chimeric antigen receptor-modified hematopoietic stem cells for cancer therapy. Hum Gene Ther 2019; 30: 413–28. [PubMed: 30860401]
16. Miletic H, Fischer Y, Litwak S, et al. Bystander killing of malignant glioma by bone marrow-derived tumor-infiltrating progenitor cells expressing a suicide gene. Mol Ther 2007; 15: 1373–81. [PubMed: 17457322]
17. Shu CJ, Guo S, Kim YJ, et al. Visualization of a primary anti-tumor immune response by positron emission tomography. Proc Natl Acad Sci USA 2005; 102: 17412–17 [PubMed: 16293690]
18. Gschweng EH, McCracken MN, Kaufman ML, et al. HSV-sr39TK positron emission tomography and suicide gene elimination of human hematopoietic stem cells and their progeny in humanized mice. Cancer Res 2014; 74: 5173–83. [PubMed: 25038231]
19. Varma NR, Shankar A, Iskander A, et al. Differential biodistribution of intravenously administered endothelial progenitor and cytotoxic T-cells in rat bearing orthotopic human glioma. BMC Med Imaging 2013; 13: 17. [PubMed: 23758888]
20. Rashidian M, Keliher EJ, Bilate AM, et al. Noninvasive imaging of immune responses. Proc Natl Acad Sci USA 2015; 112: 6146–51. [PubMed: 25902531]
21. Kim EJ, Kim S, Kang DO, Seo HS. Metabolic activity of the spleen and bone marrow in patients with acute myocardial infarction evaluated by 18F-fluorodeoxyglucose positron emission tomograpic imaging. Circ Cardiovasc Imaging 2014; 7: 454–60. [PubMed: 24488982]
22. Tavaré R, McCracken MN, Zettlitz KA, et al. Immuno-PET of murine T cell reconstitution postadoptive stem cell transplantation using anti-CD4 and anti-CD8 cys-diabodies. J Nucl Med 2015; 56: 1258–64. [PubMed: 25952734]
23. Habringer S, Lapa C, Herhaus P, et al. Dual targeting of acute leukemia and supporting niche by CXCR4-directed theranostics. Theranostics 2018; 8: 369–83. [PubMed: 29290814]
24. Van Elssen CHMJ, Rashidian M, Vrbanac V, et al. Noninvasive imaging of human immune responses in a human xenograft model of graft-versus-host disease. J Nucl Med 2017; 58: 1003–08. [PubMed: 28209904]
25. Sander WE, Metzger ME, Morizono K, et al. Noninvasive molecular imaging to detect transgene expression of lentiviral vector in nonhuman primates. J Nucl Med 2006; 47: 1212–19. [PubMed: 16818958]
26. Lee SG, Gangangari K, Kalidindi TM, Punzalan B, Larson SM, Pillarsetty NVK. Copper-64 labeled liposomes for imaging bone marrow. Nucl Med Biol 2016; 43: 781–87. [PubMed: 27694056]
27. Fiz F, Marini C, Campi C, et al. Allogeneic cell transplant expands bone marrow distribution by colonizing previously abandoned areas: an FDG PET/CT analysis. Blood 2015; 125: 4095–102. [PubMed: 25957389]

28. Marini C, Podestà M, Massollo M, et al. Intrabone transplant of cord blood stem cells establishes a local engraftment store: a functional PET/FDG study. J Biomed Biotechnol 2012; 2012: 767369. [PubMed: 23093864]
29. Inoue K, Goto R, Okada K, Kinomura S, Fukuda H. A bone marrow F-18 FDG uptake exceeding the liver uptake may indicate bone marrow hyperactivity. Ann Nucl Med 2009; 23: 643–49. [PubMed: 19629627]
30. Quarles van Ufford HM, de Jong JA, Baarslag HJ, de Haas MJ, Oud K, de Klerk JM. F-18 FDG PET in a patient with polycythemia vera. Clin Nucl Med 2008; 33: 780–81. [PubMed: 18936613]
31. Derlin T, Clauditz TS, Kröger N. (18)F-FDG PET/CT for detection of leukemic transformation in myelofibrosis. Clin Nucl Med 2015; 40: 521–22. [PubMed: 25674874]
32. Leimgruber A, Möller A, Everitt SJ, et al. Effect of platinum-based chemoradiotherapy on cellular proliferation in bone marrow and spleen, estimated by (18)F-FLT PET/CT in patients with locally advanced non-small-cell lung cancer. J Nucl Med 2014; 55: 1075–80. [PubMed: 24868108]
33. Fukuda T, Huang M, Janardhanan A, Schweitzer ME, Huang C. Correlation of bone marrow cellularity and metabolic activity in healthy volunteers with simultaneous PET/MR imaging. Skeletal Radiol 2019; 48: 527–34. [PubMed: 30194581]
34. Murata Y, Kubota K, Yukihiro M, Ito K, Watanabe H, Shibuya H. Correlations between 18F-FDG uptake by bone marrow and hematological parameters: measurements by PET/CT. Nucl Med Biol 2006; 33: 999–1004. [PubMed: 17127173]
35. Knopp MV, Bischoff H, Rimac A, Oberdorfer F, van Kaick G. Bone marrow uptake of fluorine-18-fluorodeoxyglucose following treatment with hematopoietic growth factors: initial evaluation. Nucl Med Biol 1996; 23: 845–49. [PubMed: 8940729]
36. Agriantonis DJ, Perlman SB, Longo WL. F-18 FDG PET imaging of GVHD-associated polymyositis. Clin Nucl Med 2008; 33: 688–89. [PubMed: 18806568]
37. Stelljes M, Hermann S, Albring J, et al. Clinical molecular imaging in intestinal graft-versus-host disease: mapping of disease activity, prediction, and monitoring of treatment efficiency by positron emission tomography. Blood 2008; 111: 2909–18. [PubMed: 18057227]
38. Awasthi V, Holter J, Thorp K, Anderson S, Epstein R. F-18-fluorothymidine-PET evaluation of bone marrow transplant in a rat model. Nucl Med Commun 2010; 31: 152–58. [PubMed: 19966596]
39. McGuire SM, Menda Y, Boles Ponto LL, Gross B, Buatti J, Bayouth JE. 3'-deoxy-3'-[(1)(8)F]fluorothymidine PET quantification of bone marrow response to radiation dose. Int J Radiat Oncol Biol Phys 2011; 81: 888–93. [PubMed: 21300484]
40. Williams KM, Holter-Chakrabarty J, Lindenberg L, et al. Imaging of subclinical haemopoiesis after stem-cell transplantation in patients with haematological malignancies: a prospective pilot study. Lancet Haematol 2018; 5: e44–52. [PubMed: 29248669]
41. Umeda Y, Tsujikawa T, Anzai M, et al. The vertebral 3'-deoxy-3'-^{18}F-fluorothymidine uptake predicts the hematological toxicity after systemic chemotherapy in patients with lung cancer. Eur Radiol 2019; 29: 3908–17 [PubMed: 30972546]
42. Vercellino L, Ouvrier MJ, Barré E, et al. Assessing bone marrow activity in patients with myelofibrosis: results of a pilot study of (18)F-FLT PET. J Nucl Med 2017; 58: 1603–08. [PubMed: 28360204]
43. Zade A, Purandare N, Rangarajan V, et al. Noninvasive approaches to diagnose intrathoracic extramedullary hematopoiesis: 18F-FLT PET/CT and 99mTc-SC SPECT/CT scintigraphy. Clin Nucl Med 2012; 37: 788–89. [PubMed: 22785513]
44. Agool A, Slart RH, Kluin PM, de Wolf JT, Dierckx RA, Vellenga E. F-18 FLT PET: a noninvasive diagnostic tool for visualization of the bone marrow compartment in patients with aplastic anemia: a pilot study. Clin Nucl Med 2011; 36: 286–89. [PubMed: 21368602]
45. Agool A, Schot BW, Jager PL, Vellenga E. 18F-FLT PET in hematologic disorders: a novel technique to analyze the bone marrow compartment. J Nucl Med 2006; 47: 1592–98. [PubMed: 17015893]
46. Shigematsu Y, Hirai T, Kawanaka K, et al. Distinguishing imaging features between spinal hyperplastic hematopoietic bone marrow and bone metastasis. AJNR Am J Neuroradiol 2014; 35: 2013–20. [PubMed: 24948497]

47. Kobayashi S, Saio M, Fukuda T, Kimura K, Hirato J, Oyama T. Image analysis of the nuclear characteristics of emerin protein and the correlation with nuclear grooves and intranuclear cytoplasmic inclusions in lung adenocarcinoma. Oncol Rep 2019; 41:133–42. [PubMed: 30542735]
48. Blodgett TM, Ames JT, Torok FS, McCook BM, Meltzer CC. Diffuse bone marrow uptake on whole-body F-18 fluorodeoxyglucose positron emission tomography in a patient taking recombinant erythropoietin. Clin Nucl Med 2004; 29: 161–63. [PubMed: 15162984]
49. Schelhaas S, Held A, Bäumer N, et al. Preclinical evidence that 3'-deoxy-3'-[18F] fluorothymidine PET can visualize recovery of hematopoiesis after gemcitabine chemotherapy. Cancer Res 2016; 76: 7089–95. [PubMed: 27923827]
50. Holter JL, Thorp K, Smith ML, et al. [18F]fluorothymidine PET imaging in the diagnosis of leptomeningeal involvement with diffuse large B-cell lymphoma. Cancer Imaging 2011; 11: 140–43. [PubMed: 22004872]
51. Williams KM, Hakim FT, Gress RE. T cell immune reconstitution following lymphodepletion. Semin Immunol 2007; 19: 318–30. [PubMed: 18023361]
52. Miletic H, Fischer YH, Giroglou T, et al. Normal brain cells contribute to the bystander effect in suicide gene therapy of malignant glioma. Clin Cancer Res 2007; 13: 6761–68. [PubMed: 18006778]
53. Keu KV, Witney TH, Yaghoubi S, et al. Reporter gene imaging of targeted T cell immunotherapy in recurrent glioma. Sci Transl Med 2017; 9: eaag2196. [PubMed: 28100832]
54. Rashidian M, Keliher E, Dougan M, et al. The use of ^{18}F-2-fluorodeoxyglucose (FDG) to label antibody fragments for immuno-PET of pancreatic cancer. ACS Cent Sci 2015; 1: 142–47. [PubMed: 26955657]
55. Kawano T, Suzuki A, Ishida A, et al. The clinical relevance of thymic fluorodeoxyglucose uptake in pediatric patients after chemotherapy. Eur J Nucl Med Mol Imaging 2004; 31: 831–36. [PubMed: 14963698]

Search strategy and selection criteria

We did a MEDLINE search on July 5, 2019, for all papers published with the following search terms: “haematopoietic” and “positron emission tomography”; this search returned 313 papers published from Aug 1996 to July 2019. Papers were excluded as follows: non-English (n=2), not involving the search terms (n=122), editorials, reviews, and articles not published in peer reviewed journals (n=45), subject area was primary extra medullary malignancies or infection, as these topics had been reviewed elsewhere and not relevant to this Viewpoint (n=73). Multiple search terms were attempted to yield the greatest number of relevant papers for inclusion. As few patients are included in these studies and few animal model studies have been verified by multiple groups, the strength of these data are low to influence medical choices. Thus, this Viewpoint describes emerging research opportunities for the role of nuclear medicine to evaluate the process of haemopoietic stem cell transplantation, rather than grading the evidence or promoting use of these technologies.

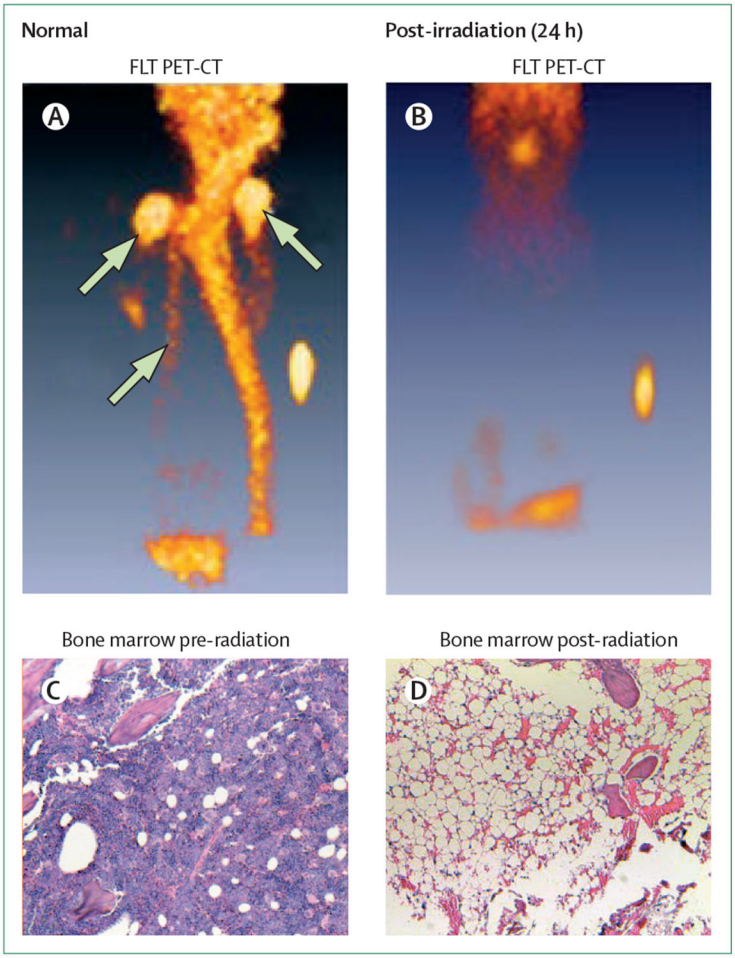

Figure 1: Radiation marrow depletion

Imaged by ^{18}F-FLT PET-CT in Wistar-furth rats at baseline (normal; A), at 24 h after 950 cGy by caesium source (sample aliquot for calibration visualised; B). Haematoxylin and eosin stained bone marrow biopsy done at baseline (C) and after myeloablated radiation (D), confirming that the ^{18}F-FLT images of marrow absence reflect cellular aplasia. The top two white arrows indicate left and right humeri, and the lower white arrow represents the sternum. Reproduced from Awasthi and colleagues,[12] by permission of Lippincott Williams (SAGE Publishing). ^{18}F-FLT=^{18}F-fluorothymidine.

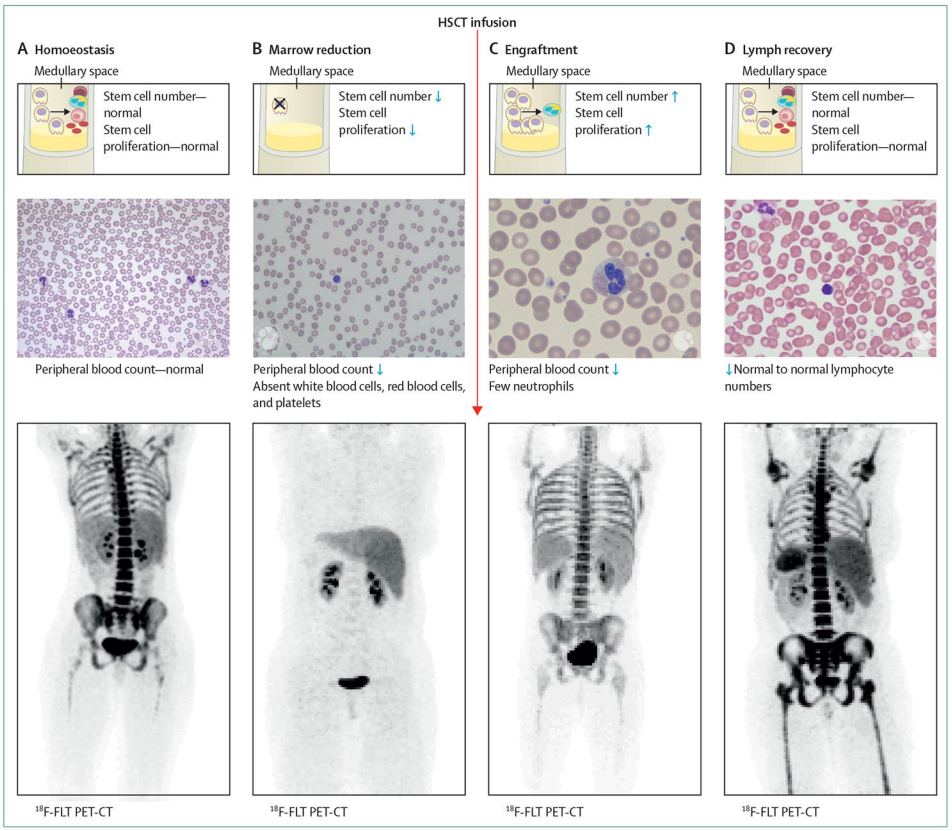

Figure 2: Phases of HSCT

In homoeostasis (A), cell production, cell number, and associated normal peripheral blood count are normal. The image used for the ^{18}F-FLT is from a patient 1 year after their transplant when normal homoeostasis in the axial skeleton had returned. In the marrow reduction phase (HSCT preparative phase; (B), the cell number and proliferation in the marrow is reduced and the peripheral counts are reduced. ^{18}F-FLT image following myeloablation shows this phase. (C) Engraftment (includes subclinical engraftment followed by clinical engraftment with peripheral neutrophils). Neutrophils and natural killer cells recover first in the periphery, followed by other cell populations.[51] The medullary space shows rapid haemopoietic stem cell division and early differentiation into neutrophils. The peripheral blood shows predominantly neutrophils and the ^{18}F-FLT PET-CT image is from 9 days after myeloablative HSCT, in a time of subclinical engraftment. (D) Lymph recovery, characterised by expansion of infused lymphocytes and then de novo production of T cells in the thymus and de novo production of B cells in the marrow. This final phase of HSCT begins in the first month after transplantation, continuing for years. The image shown by ^{18}F-FLT PET-CT is at 28 days after HSCT. Medullary spaces are depicted with the stem cells (yellow cells with large single nucleus), differentiating into platelets (small brown-red cells), red blood cells (pink cell, red centre, as shown in panel A and D), neutrophils (yellow cell with multiple blue nuclei), and lymphocytes (purple cell with single nucleus). Blue arrows represent represent increased and decreased levels. Reproduced from Williams and colleaguesl[40] by permission of Elsevier. ^{18}F-FLT=^{18}F-fluorothymidine. HSC=haemopoietic stem cell. HSCT=haemopoietic stem cell transplantation.

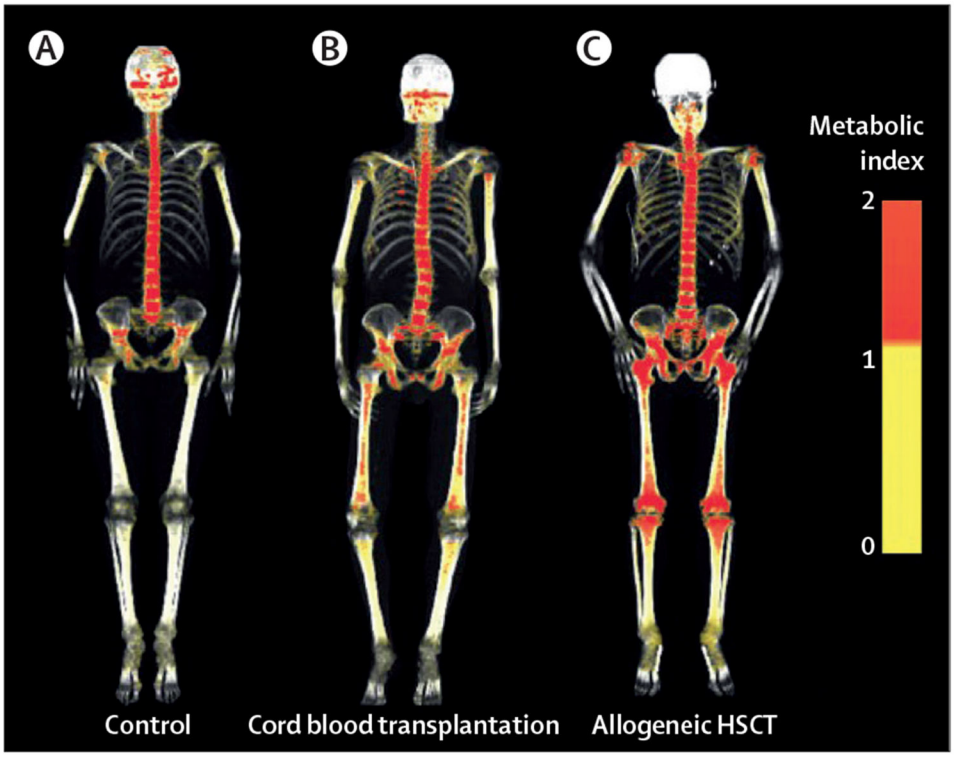

Figure 3: ^{18}F-FDG (fluorodeoxyglucose) three-dimensional reconstructions of the skeleton following cord blood or allogeneic HSCT

A control adult with marrow homoeostasis in their axial skeleton is shown on the left (A), followed by an individual who underwent cord blood transplantation 1 month before this image with heterogeneous uptake of marrow spaces, including extremities (B). The cord blood transplant recipient is less metabolic active than the allogeneic marrow or peripheral transplant recipient at the same time after transplantation (C). Reproduced from Fiz and colleagues,[27] by permission of Blood (American Society of Hematology). SUV=standardised uptake volume.

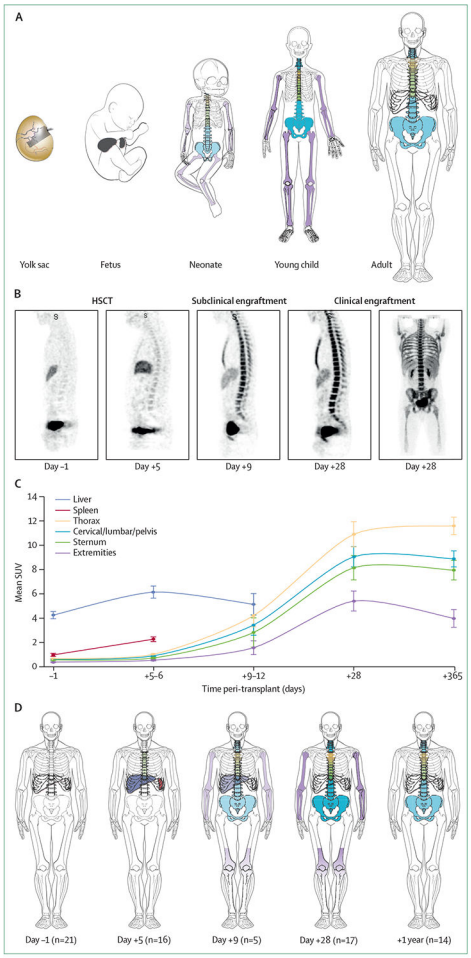

Figure 4: ^{18}F-FLT pattern of subclinical cellular settling after HSCT that recapitulates fetal ontogeny

(A) Pattern of fetal ontogeny. (B) ^{18}F-FLT PET-CT images during HSCT. ^{18}F-FLT PET-CT was done 1 day before allogeneic HSCT after myeloablation (done on day–1 of HSCT), followed by images of subclinical engraftment (done on days 5–9 after HSCT), followed by images after clinical engraftment (3 consecutive days of neutrophil peripheral count ≥500 cell/dL). Uptake in medullary spaces shows increasing marrow proliferation over time after HSCT. (C) Means (SEs) of median SUVs for each organ, based on data from 21 HSCT recipients imaged with ^{18}F-fluorothymidine, and (D) pattern of HSC engraftment in these patients. Because the sternum overlies the thoracic spaces, only the upper one-third is coloured and the thoracic vertebral bodies are shown in the position of the lower two-thirds. Splenic uptake reflected secondary lymphoid expansion after day 28 and, therefore, these data were included only up to day 28. HSCT=haemopoietic stem-cell transplantation. SUV=standardised uptake value. Reproduced from Williams and colleagues,[40] by permission of Elsevier.

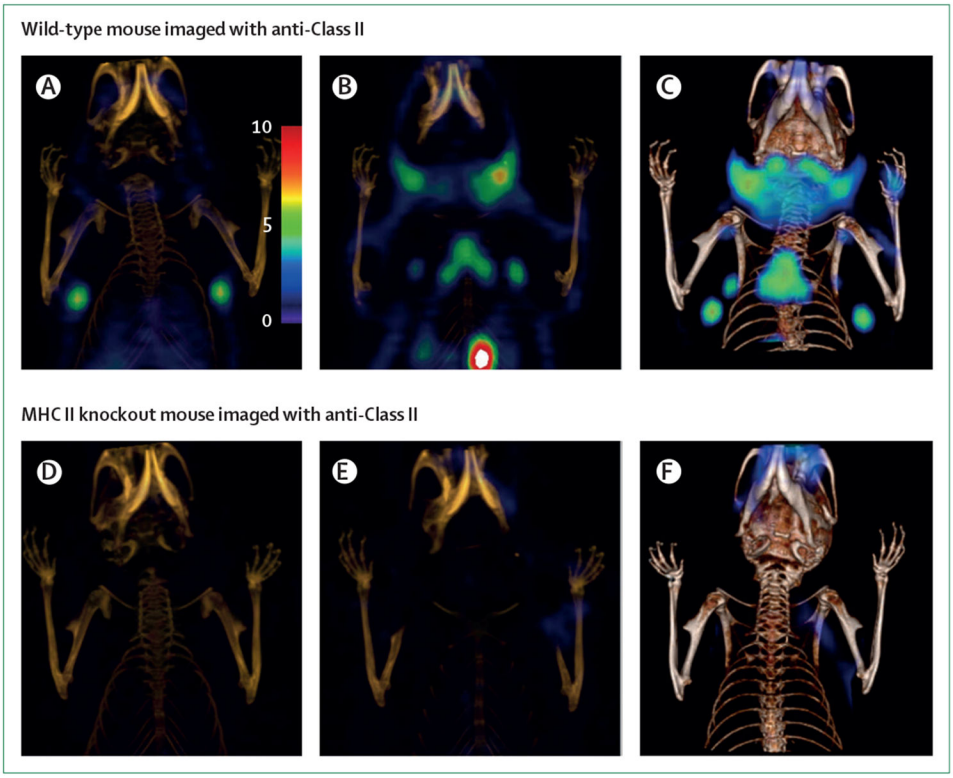

Figure 5: Imaging MHC-class II activity by PET-CT

PET-CT images of C57BL6 mice treated with ^{18}F-labelled minibodies targeting MHC-class II anterior to posterior (A–F). Lymphoid cells express MHC-class II, thus the primary and secondary lymphoid organs show increased minibody uptake in wild-type mouse (A–C). Specificity of the minibody is shown by the absence of uptake in the MHC ii knockout murine model (D-F). Reproduced from Rashidian and colleagues,[54] by permission of ACS publications. WT=wild type.

Table:

Radioisotopes used in human and animal models of haematopoietic stem cell transplantation

	Cell labelled	Human or animal	Metabolic, proliferative, or static	Potential clinical uses	Reference
^{18}F-L-FMAU + *hdCK3mut* (in vitro label—uracil analogue)	HSCs and progeny	Animal	Proliferative	Tracking and durability of engraftment after HSCT	McCraken et al (2013)[4]
HSV1-TK-EGFP-FLuc TGL (in vitro label—thymidine analogue)	HSCs	Animal	Proliferative	Proliferation of HSCs post-transplant and sites of early engraftment	Mayer-Kucuck et al (2006)[5]
^{18}F-FDG-labelled HSC (in vitro label—glucose metabolism)	HSCs	Animal	Metabolic	None (toxic to the HSCs)	Faivre et al (2016)[6]
^{89}Zr + protamine-labelled HSC (in vitro label—passive diffusion)	HSCs	Animal	Static	Identify early HSC settling	Pantin et al (2015)[7]
HSV1-TK + ^{18}F-FIAU-labelled HSC (in vitro label—uracil analogue)	HSCs	Animal	Proliferative	Identify transfected HSC proliferation	Pei et al (2012)[8]
^{64}Cu-PTSM (in vitro label—copper metabolism)	HSCs and mesenchymal stem cells	Animal	Static	Identified cells in vitro	Huang et al (2008)[9]
^{18}F-AraG (in vivo—guanosine analogue)	T cells and T lymphoblastoid cells in GVHD	Animal	Proliferative	Identifies activated T cells and induces lysis	Ronald et al (2017)[10]
^{18}F-FLT (in vivo—thymidine analogue)	T cells in GVHD	Animal	Proliferative	Marrow activity; increased uptake in secondary lymphoid organs before development of GVHD; sites of initial marrow settling influenced by radiation exposure	Lee et al (2018);[11] Afshar et al (2017);[12] Rowe et al (2013)[13]
^{18}F-FDG (in vivo—metabolism of glucose)	Marrow cells	Animal	Metabolic	Detects marrow loss after radiation	Chen et al (2012)[14]
^{18}F-L-FMAU + *hdCK3mut* with T-cell receptor to F5 (in vitro label—uracil analogue)	Transduced T cells	Animal	Proliferative	Homing and cytotoxicity *vs* melanoma	McCraken et al (2013)[4]
^{89}Zr-labelled cetuximab, CD19 CAR + EGFRt (in vitro label—inhibitor to EGFRt)	Transduced T cells	Animal	Static	Detects labelled immunotherapy T cells	Kao et al (2019)[15]
HSV1-TK – ^{18}F-FHBG (in vitro label—thymidine analogue)	Transduced T cells	Animal	Proliferative	Detects T cells that home to tumors	Miletic et al (2007),[16] Shu et al (2005)[17]
HSV1-TK – ^{18}F-FHBG + NYO-ESO1 (in vitro label—thymidine analogue)	Transduced T cells	Animal	Proliferative	Detects T cells that home to melanoma	Gschweng et al (2014)[18]
^{111}In is passively absorbed and trapped in T cells (in vitro)	Cytotoxic T cells	Animal	Static	Detects T cells that home to tumour and T-cell density	Varma et al (2013)[19]
^{64}Cu, or ^{18}F minibody *vs* MHC II and CD11b (in vivo—MHC II and CD11b)	Dendritic cells and macrophages	Animal	Static	Detects influx of antigen presenting cells to tumour	Rashidian et al (2015)[20]
^{18}F-clofarabine (in vivo—clofarabine)	Marrow and lymphoid cells	Animal	Proliferative	Detects marrow and lymphoid cells after radiation therapy	Kim et al (2015)[21]

Lancet Haematol. Author manuscript; available in PMC 2021 March 01.

	Cell labelled	Human or animal	Metabolic, proliferative, or static	Potential clinical uses	Reference
^{89}Zr by passive uptake (in vitro)	T cells	Animal	Static	Detects primary and secondary lymphoid recovery	Tavaré et al (2015)[22]
^{68}Ga labelled plexifor (CXCr4 substrate; in vitro)	CXCR4+ leukaemia cells	Animal	Static	Detects leukaemia burden	Habringer et al (2018)[23]
^{64}Cu minibody *vs* HLA-DR (in vivo—copper metabolism)	T cells	Animal	Static	Lymphoid organ uptake in subclinical GVHD	Van Elssen et al (2017)[24]
TK mutant transfected with PET reporter ^{76}B-FBAU	CD34+ cells	Animal	Static	Identify marrow toxicity	Sanders et al (2006)[25]
^{64}Cu-liposome (in vitro label—liposome delivery)	Marrow	Animal	Static	Marrow activity	Lee et al (2016)[26]
^{18}F-FDG (in vivo—glucose metabolism)	Marrow cells	Human	Metabolic	Identifies marrow activity; marrow reserve; influence of medication on marrow activity; sites of marrow settling and activity after HSCT; infiltrative leukaemia in myelofibrosis; marrow loss after chemotherapy or radiation; sites of marrow inflammation; increased uptake in GVHD; return to normal marrow following allogeneic transplantation for myelofibrosis	Fiz et al (2015);[27] Marini et al (2012);[28] Inoue et al (2009);[29] Quarles et al;[30] Derlin et al;[31] Leimgruber et al (2014);[32] Fukuda et al (2019);[33] Murata et al (2006);[34] Knopp et al (1996);[35] Argiantonis et al;[36] Stelljes et al (2008);[37] Derlin et al[31]
^{18}F-FLT (in vivo—thymidine)	Marrow cells	Human	Proliferative	Sites of marrow settling and activity after HSCT; identifies marrow loss after chemotherapy, level of fibrosis in myelofibrosis, extramedullary haemopoiesis, increased FLT in stimulated marrow with myelodysplasia, and differentiates myelofibrosis and aplastic anaemia	Awasthi et al (2010);[38] Mcguire et al (2011);[39] Williams et al (2018);[40] Umeda et al (2019);[41] Vercellino;[42] Zade et al (2012);[43] Inoue et al (2009);[29] Agool et al (2011);[44] Agool et al (2006)[45]
^{68}Ga labelled plexifor (CXCr4 substrate; in vitro)	CXCR4+ leukaemia cells	Human	Static	Detects leukaemia burden	Habringer et al (2018)[23]
^{18}F-FDG MRI and CT (in vivo—glucose metabolism)	Hyperplastic haemopoiesis bone marrow *vs* spinal metastasis	Human	Metabolic	Distinguishes between marrow cells *vs* metastatic disease	Shigematsu et al (2014)[46]

The first column of the table lists the radiolabel and (in parentheses) whether it is an in vitro label or in vivo followed by the target of the radioisotope. ^{76}Br-FBAU=5-^{76}Br-bromo-2-fluoro-2-deoxyuridine. CD19 CAR=CD19 chimeric antigen receptor. ^{64}Cu-PTSM=^{64}Cu-pyruvaldehyde-bis(N4-methylthiosemicarbazone). EGFRt=truncated EGFR. ^{18}F-AraG=2′-deoxy-2′-[^{18}F]-fluoro-9-β-D-arabinofuranosylguanine. ^{18}F-FDG=^{18}F-fluorodeoxyglucose. ^{18}F-FIAU=2′-deoxy-2′-18F-fluoro-5-iodo-1-β-D-arabinofuranosyluracil. ^{18}F-FHBG=4-[^{18}F]-fluoro-3-hydroxymethylbutyl-guanine. ^{18}F-FLT=^{18}F-fluorothymidine. ^{18}F-L-FMAU=1-(2-deoxy-s-[^{18}F]-fluoro-β-L-arabinofuranosyl)-5-methyluracil. GVHD=graft-versus-host disease. HSC=haemopoietic stem cell. HSCT=haemopoietic stem cell transplantation. HSV1-TK=mutant viral herpes simplex virus type 1-thymidine kinase gene. HSV1-TK-EGFP-FLuc TGL=HSV1-TK-enhanced green fluorescence protein-firefly luciferase triple gene reporter. NYO-ESO1=New York esophageal squamous cell carcinoma 1.